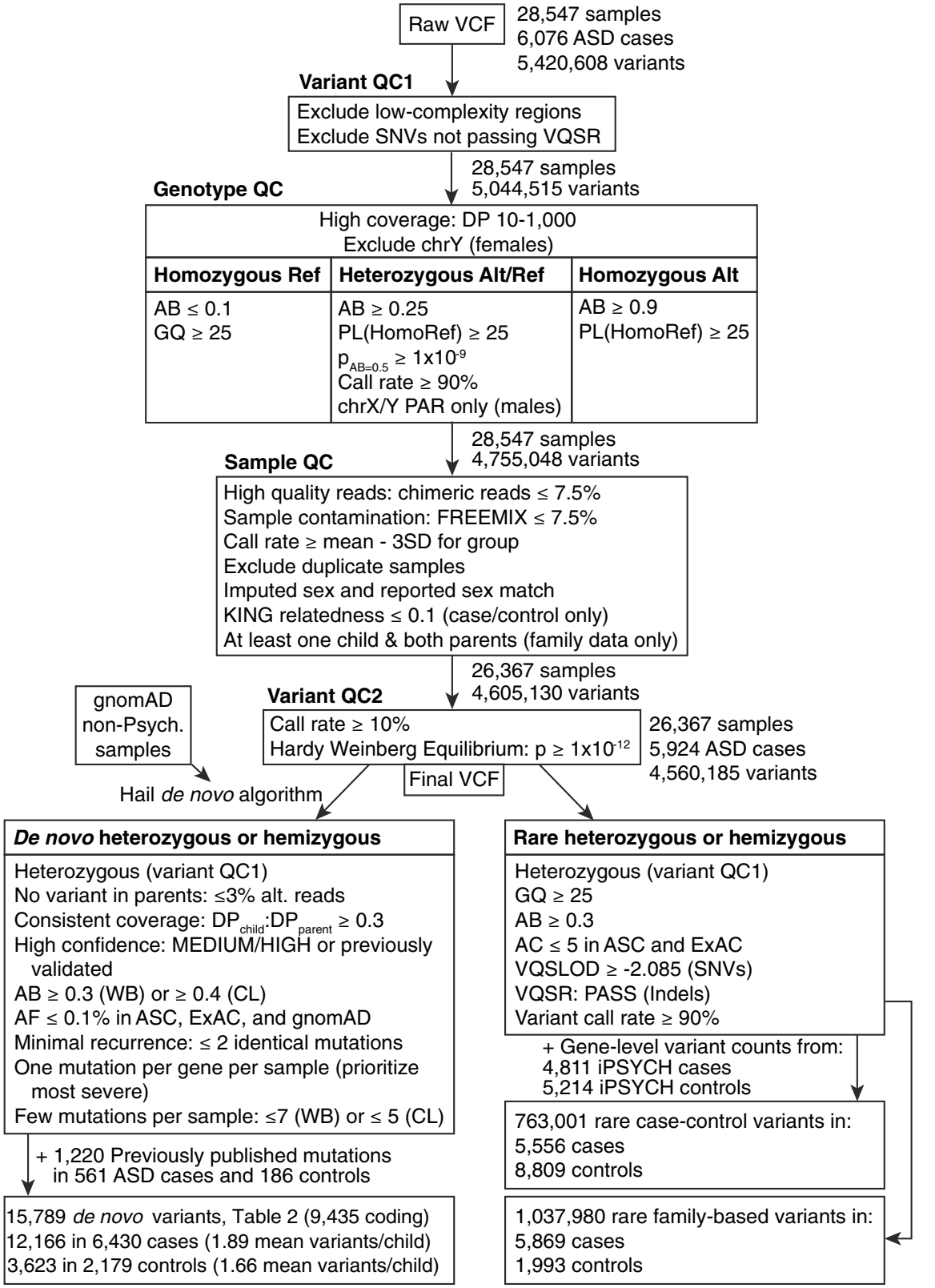

(legend on next page)

Figure S1. Data Processing for Samples with Read-Level Exome Data, Related to Figure 1

This figure describes the variant, genotype, and sample quality control steps that were applied to the raw joint-genotyped variant calls (VCF) to generate the *de novo*, case-control, and inherited variants used in downstream analyses. Low-complexity regions were defined by Li (2014). VQSR, estimated chimeric reads, and estimated contamination were calculated by the Genome Analysis Toolkit (GATK); relatedness values were calculated by KING (Manichaikul et al., 2010); most data handling occurred in Hail 0.1 (http://hail.is; https://github.com/hail-is/hail). Metrics from ExAC and gnomAD were used to exclude common variants. Abbreviations: VCF: Variant Call Format; QC: Quality control; VQSR: Variant Quality Score Recalibration; DP: read depth; AB: allele balance; GQ: genotype quality; PL: Phred-scaled likelihood of the genotype; PAR: pseudoautosomal region; SD: standard deviation; WB: whole-blood derived DNA; CL: cell-line derived DNA; AF: allele frequency; AC: allele count; VQSLOD: variant quality score log-odds.

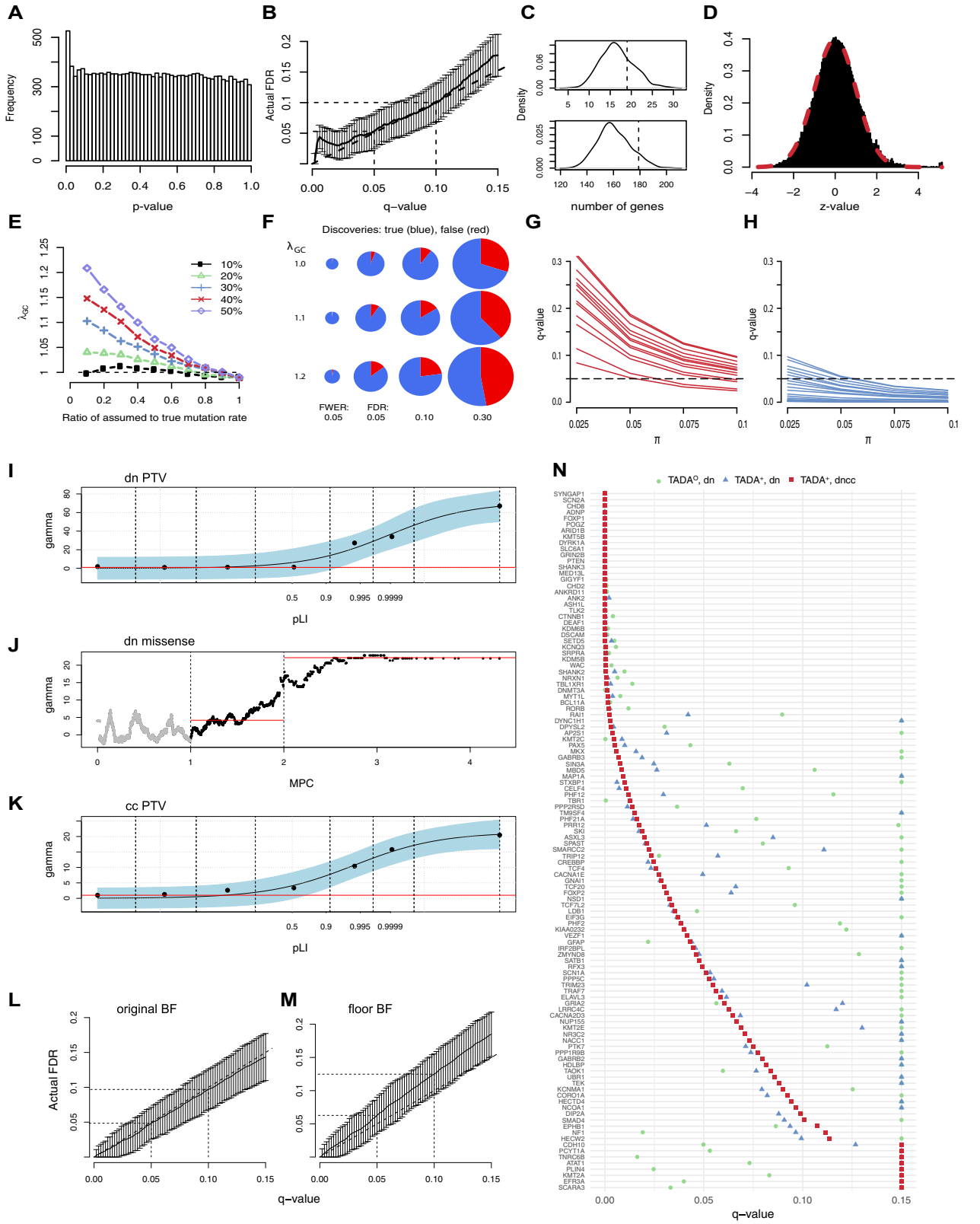

(legend on next page)

Figure S2. Enhancing the TADA Model and Evaluating Its Accuracy, Related to Figure 2

A) Distribution of p-values from the TADA analysis of protein truncating variants (PTVs) and Mis3 (PolyPhen-2 probably damaging) variants in the data. B) Empirical-known signal experiments (EKSE) to evaluate the control of FDR. The bold line shows the FDR, averaged over 20 iterations versus q-values. For these iterations, a true signal is superimposed on a common background of benign mutations. Error bars are obtained from the "pure" simulation (STAR Methods). C) Observed vs. simulated distribution of synonymous and Mis1 (PolyPhen-2 benign) variants. The solid line shows the distribution of 500 simulation results, compared to the observed shown in the dashed line. Top: the number of genes with synonymous events ≥ 3. The average over simulations is 16.6, while the observed is 19. Bottom: the number of genes with Mis1 (PolyPhen-2 benign) events ≥ 2. The average over simulations is 160.6, while the observed is 179. D) To visualize potential deviations from the model in the TADA analysis of the true ASD sample, TADA p-values are converted to z-values, which are assumed to follow a standard normal density (for null genes). Here a normal density with mean zero and variance = 1.02 (in red) is superimposed on the histogram of results from the real data, illustrating how closely the data follow the assumed model (1.02 = variance = λGC for these results). E) Underestimating the per-gene mutation rate could lead to false discoveries. To assess the impact of model misspecification, the genomic control factor, λGC, is plotted for various misspecifications of μ. Each line corresponds to a different fraction of genes with underestimated μ, and the x-axis is the magnitude of the underestimation: μused /μtrue. F) True discoveries (TD) and false discoveries (FD) by critical value, and for various levels of model discrepancy, with λ_{GC} as the genomic control factor. FWER is set at the correction rate. FDR is set at 0.05, 0.10, and 0.30. The circumference of each pie chart equals the cube root of the total number of discoveries. We observe that the q-values of both non-signal (G) and signal (H) borderline genes decreases as π increases, but the impact on the non-signal borderline genes is not substantial and q-values for only a few of these genes cross the threshold. I) The average relative risk (γ) for variants in the data. We model the relative risk for *de novo* protein truncating variants (PTVs) as a continuous function of pLI. J) For *de novo* missense variants, we estimate the curve using a moving window over probands' missense variants ordered by MPC score. The MPC score can be cut into three categories, and we use the last two in the TADA analysis, since γ in the first category is close to the null value of one. K) For case-control PTVs, we model the relative risk as a continuous function of pLI. L) The empirical FDR versus q-values, averaged over 100 simulations using the original Bayes Factors. M) The empirical FDR versus q-values, averaged over 100 simulations using the Bayes Factors with a lower limit. N) The q-values for three types of TADA analyses. We present the 114 genes with q-value less than 0.1 in at least one analysis.

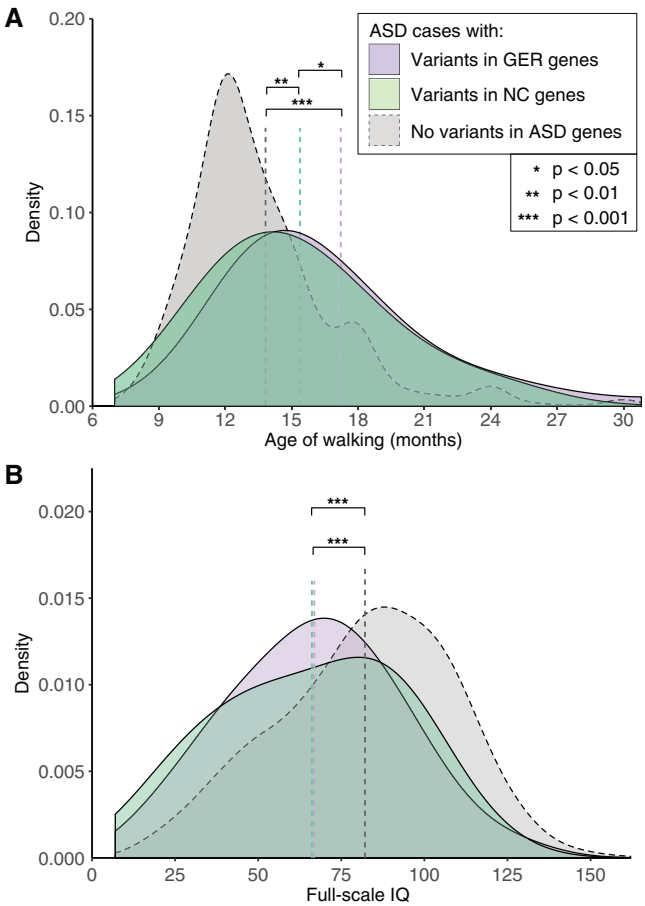

Figure S3. Phenotypic Distribution of Age of Walking and FSIQ in ASD Individuals, Split by Those Carrying *De Novo* Variants in GER Genes and NC Genes, Related to Figure 3

A) Age of walking distribution for 4,456 ASD probands for whom age of walking data was available split into three groups: those carrying a *de novo* missense (MPC $\geq$ 1) variant or PTV in a GER gene (N=140, purple), those carrying a *de novo* missense (MPC $\geq$ 1) variant or PTV in an NC gene (N=71, green), and the rest of the ASD population without such a *de novo* variant in the 102 FDR<0.1 genes (N=4,204, grey). B) Full-scale IQ (FSIQ) distribution for 4,821 ASD probands for whom FSIQ was available split into three groups: those carrying a *de novo* missense (MPC $\geq$ 1) variant or PTV in a GER gene (N=159, purple), those carrying a *de novo* missense (MPC $\geq$ 1) variant or PTV in an NC gene (N=77, green), and the rest of the ASD population without such a *de novo* variant in the 102 FDR<0.1 genes (N=4,542, grey).

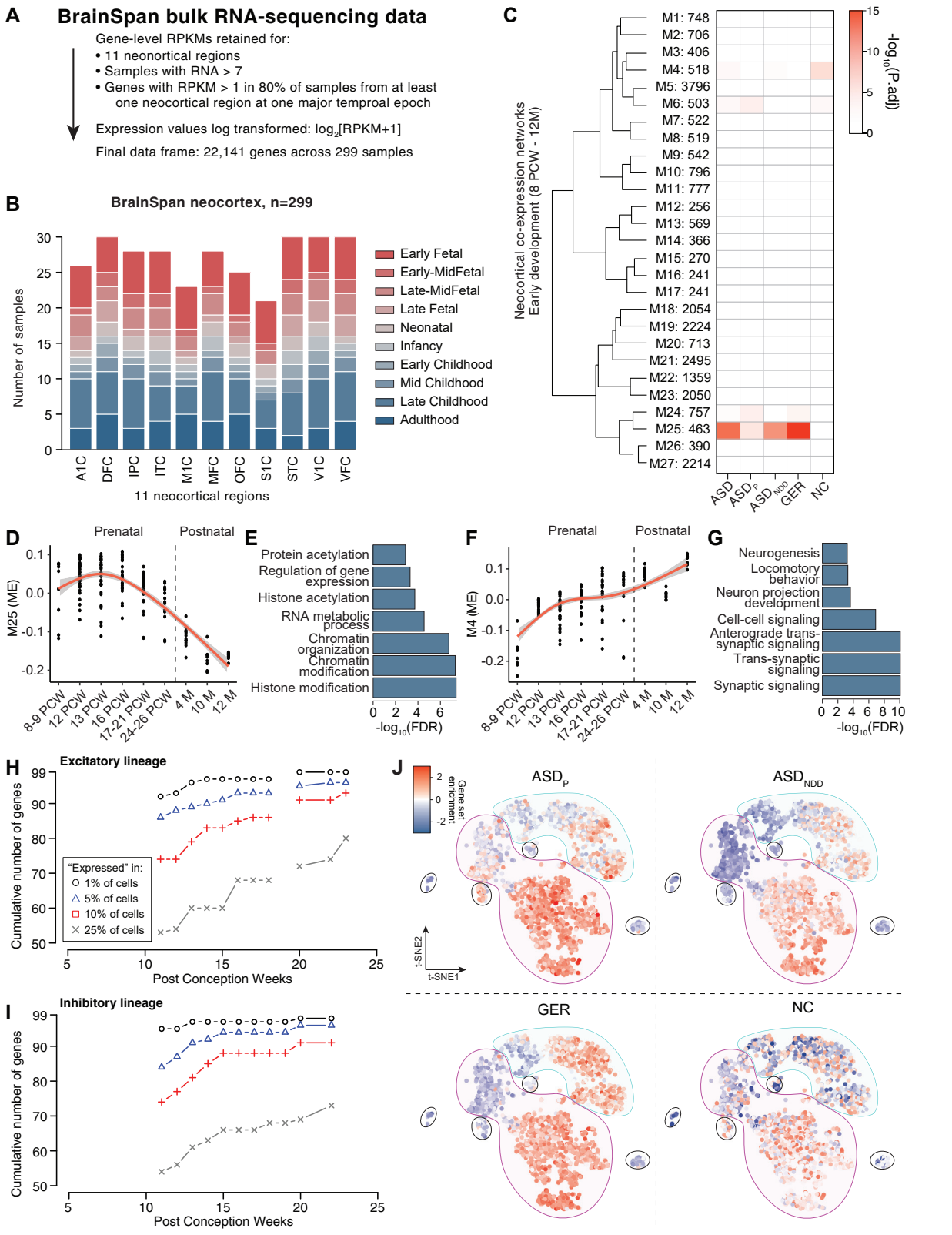

(legend on next page)

Figure S4. Enrichment of 102 ASD Genes in WGCNA Modules from Human Cortex and in Single-Cell Gene Expression Data, Related to Figure 5

A) BrainSpan bulk RNA-sequencing data underwent extensive data quality control and data pre-processing. B) A total of 299 postmortem brain samples were used to assess prenatal versus postnatal bias in gene expression patterns for each individual gene. C) Next, a subset of 177 high-quality samples aged 8 postconception weeks (pcw) to 1 year of age were used to construct early developmental coexpression networks (i.e. modules). A total of 27 modules were identified, clustered by module eigengene (ME) values and assessed for enrichment for the 102 ASD risk genes and selected functional subsets. Node color intensity indicates significance level. Module number and the total number of genes within each module are labeled to the right of the enrichment plot. Splines were applied to capture non-linear ME effects while ensuring patterns of gene expression are continuous across early development. D) Peaking in expression during mid-fetal development, module M25 was enriched for ASD and GER genes and E) was enriched for chromatin modification/organization and histone modification/acetylation terms. F) Peaking in expression during neonatal/infancy, module M4 was enriched for NC genes and G) was implicated in transsynaptic signaling and cell-cell signaling. H) The cumulative number of ASD-associated genes expressed in RNA-seq data for different definitions of expression (0.01-0.25 of cells contain at least one transcript of the gene) and for 4,261 cells collected from human forebrain across prenatal development (Figure 5D) in all cells from the excitatory lineage. I) The plot in 'H' is repeated for all cells in the inhibitory lineage. J) The enrichment of ASD associated genes in single cells arranged using tSNE (Figure 5F) divided into the ASDP, ASDNDD, GER, and NC gene sets.

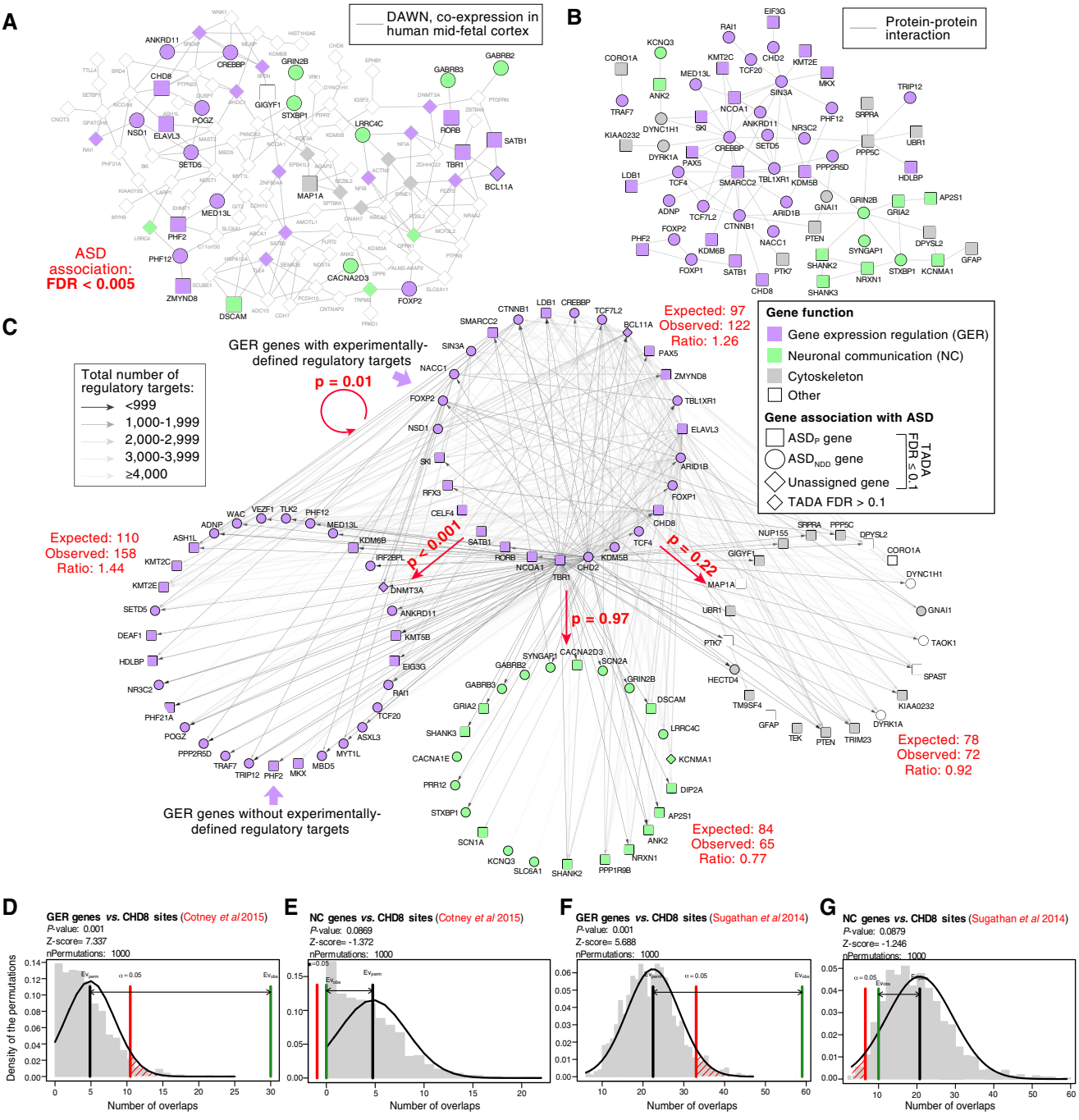

Figure S5. Functional Relationships of ASD Risk Genes, Related to Figure 5

A) ASD association data from TADA (Table S2) is integrated with co-expression data from the midfetal human brain to implicate additional genes in ASD using DAWN (Discovering Association With Networks). The top 138 genes that share edges are shown (FDR $\leq$ 0.005). B) ASD-associated genes form a single protein-protein interaction network with more edges than expected by chance (p=0.01 using permutation). C) Experimental data, obtained using ChIP and CLIP methods across multiple species and a wide range of neuronal and non-neuronal tissues types, identified the regulatory targets of 26 GER genes (top circle). These data were used to assess whether three functionally defined groups of ASD-associated genes were enriched for regulatory targets, represented as arrows, weighted by the total number of regulatory targets for the GER genes. The expected number of targets in each functional group was estimated by permutation, controlling for brain expression, de novo PTV mutation rate, and pLI. For CHD8 enrichment analysis, genomic coordinates for GER and NC genes were assessed for enrichment for human brain-specific CHD8 binding sites derived from (D-E) human mid-fetal brain tissue and (F-G) human neural progenitor cells (NPCs). The regioneR R package was used to test overlaps of genomic regions based on permutation sampling. We sampled random regions from the genome 1,000 times, matching size and chromosomal distribution of the region set under study. By recomputing the overlap with CHD8 binding sites in each permutation, statistical significance of the observed overlap was computed. We observed significant enrichment for GER genes and CHD8 binding sites derived from (D) human midfetal brain tissue and (F) human NPCs. However, no significant enrichment was observed for NC genes from either study.